Influence of Current Ripples in Cascaded Multilevel Topologies on the Aging of Lithium Batteries

Fengqi Chang, Felix Roemer, *Student Member, IEEE*, and Markus Lienkamp

***Abstract*—Previous studies have proposed to use cascaded multilevel topologies in stationary battery energy storage systems (BESSs) or in BESSs of electric vehicles, due to the balancing capability or the high efficiency of these topologies. Because of the elimination of the direct current (dc) bus, the batteries in these topologies are expected to experience large current ripples. However, whether these current ripples can accelerate the aging of the batteries has not yet been dedicatedly investigated, although it is a determining factor for the feasibility of this category of topologies. Therefore, this article first summarizes the existing studies regarding the influence of current ripples on the aging of lithium batteries, which proves the necessity of an experimental investigation. Then, a long-term aging experiment on battery cells is conducted, in order to examine the influence of the current ripples in cascaded multilevel topologies. According to the experimental results and the conclusions in previous studies, the ripples in cascaded multilevel topologies generally have a negligible influence on the aging of batteries, except in certain scenarios. These scenarios can be identified by the three preconditions, first, current ripples must contain micro charge and discharge cycles; second, the microcycles are below 10 Hz; third, low frequency microcycles must contribute a large amount of charge throughput.**

***Index Terms*—Battery aging, electric vehicles, energy storage, multilevel converter, ripple current.**

NOMENCLATURE

$\cos\theta$	Power factor of the cascaded multilevel topology.
I_{ACpeak}	Peak value of the phase ac current.
$I_{\mathrm{bat\_ave}}$	Average value of the battery current.
$I_{\mathrm{bat\_RMS}}$	RMS value of the battery current.
$I_{\mathrm{ripple\_RMS}}$	RMS value of the ripple components in the battery current.
$I_{\mathrm{Q\_Mcycle}}$	Charge throughput rate caused by the microcycles in ripples.
i_{bat}	Current of the battery.
m_{a}	Modulation index of the topology.
N	Carrier index of the topology.
T_{AC}	AC output period of the cascaded multilevel topology.
T_{S}	Switching period of the cascaded multilevel topology.
U_{ACpeak}	Peak value of the phase ac voltage.

Manuscript received November 26, 2019; revised February 29, 2020; accepted April 14, 2020. Date of publication April 19, 2020; date of current version July 20, 2020. This work was supported by the Singapore National Research Foundation under its Campus for Research Excellence and Technological Enterprise programme. Recommended for publication by Associate Editor L. Dalessandro. *(Corresponding author: Fengqi Chang.)*

Fengqi Chang is with the Institute of Automotive Technology, Technische Universitat Munchen Fakultat fur Maschinenwesen, 85748 Garching, Germany (e-mail: fengqi.chang@tum-create.edu.sg).

Felix Roemer is with the IMVS, TUMCREATE, 138602, Singapore (e-mail: felix.
roemer@tum-create.edu.sg).

Markus Lienkamp is with the Institute of Automotive Technology, Technical University of Munich, 80333 Munich, Germany (e-mail: lienkamp@ftm.mw.tum.de).

Color versions of one or more of the figures in this article are available online at https://ieeexplore.ieee.org.

Digital Object Identifier 10.1109/TPEL.2020.2989145

I. INTRODUCTION

SINCE renewable energy and electric vehicles (EVs) start to be accepted by the general public in recent years, battery energy storage system (BESS) has become one of the main research topics in the field of power electronics [1]–[9]. Stationary BESSs are deemed by many researchers as the ultimate solution to damp the fluctuations of solar or wind power in the power grid, and the topologies or controlling algorithms of stationary BESSs have attracted extensive efforts of research [8]–[13]. Different topologies and controlling algorithms are also proposed to optimize the management or the utilization of the batteries in EVs [14]–[18] (hereafter referred as on-board BESSs), as the on-board BESSs still account for the most significant part in the total cost of EVs [19], [20]. Among all the topologies for BESSs, the cascaded multilevel topologies with an alternative current (ac) interface were proved to be one of the most promising options for both on-board and stationary BESSs, due to the advantages in terms of modularity [21], [22], state-of-charge (SOC) balancing [22]–[24], and cost and efficiency [14], [24]. A typical example of this kind of topologies is the cascaded H-Bridge (CHB), as shown in Fig. 1. Instead of connecting all the battery cells together to form a dc bus, these topologies distribute the battery cells in many power conversion submodules. The submodules are H-bridges in a CHB topology, as shown in Fig. 1. Submodules are then cascaded to directly generate ac voltage required by the load. This type of topology has been proposed by several studies to use in EVs [14], [24].

However, due to the elimination of the dc bus in these topologies, the batteries are only supplying power for a single phase. As a result, the current of the battery cells contains large ripples that are commonly visible on the dc bus of single-phase systems, e.g., uninterruptible power supplies and on-board chargers [25], [26]. The current waveform of one battery cell measured in a CHB topology is depicted in Fig. 2, where positive current implies the discharge of the battery cell. The battery current in a variety of other cascaded multilevel topologies has the same pattern. The

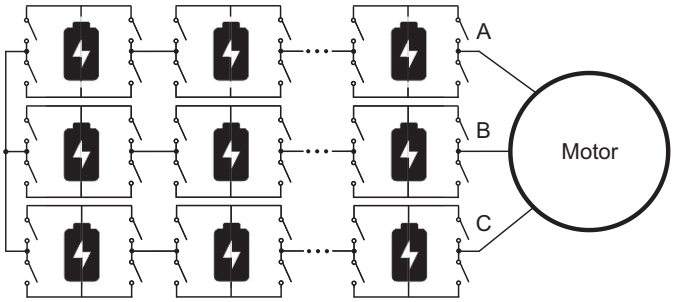

Fig. 1. CHB for EVs.

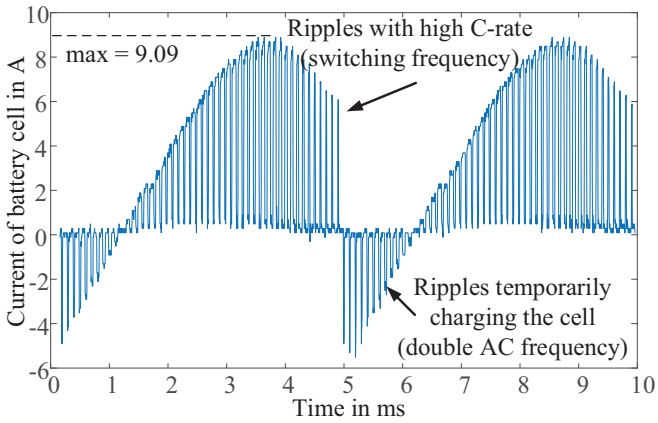

Fig. 2. Current waveform of one battery cell in a CHB circuit, when the power factor is 0.8.

current of the battery contains ripples in double ac frequency and ripples in switching frequency. The switching frequency ripples in the current are generated by the pulsewidth modulation (PWM) process, because the batteries are directly connected to the switches. The double ac frequency ripples are caused by the intrinsic characteristics of single phase system. Further, when the power factor is not strictly 1.0, negative current also appears in the waveform [25]. From a conventional perspective, both types of ripples might be able to accelerate the aging of lithium batteries.

First, the switching frequency ripples might be able to accelerate the aging, because of their high C-rate, which is identified as a driving factor for battery aging in multiple studies [25], [26]. In Fig. 2, the average discharge current is only 2.4 A, but the peak value of the switching frequency ripples is 9.09 A. Such a high peak value is only instantaneous. However, it is not certain if the repetitive instantaneous high current ripples in switching frequency are harmful to battery cells. Second, due to the double ac frequency ripples, the battery cells in the CHB will be temporarily charged, while the CHB is discharging to the load. Compared to the cells discharged by dc current, the double ac frequency ripples create micro charge and discharge cycles, and thus increase the charge throughput of cells. As the charge throughput is proven to be one of the most significant driving factors for the battery aging [27]–[30], the double ac frequency ripples may also be harmful to batteries. The cycle life of battery cells might be consumed much faster in the CHB, due to the existence of the microcycles.

Because of the concerns over the two types of current ripples, before implementing multilevel topologies in BESSs, it is necessary to investigate the impacts of the ripples in Fig. 2 on the aging of lithium batteries. If identified to be significantly harmful to lithium batteries, these topologies should be reconsidered, especially for BEVs. In this article, the ripple current in the CHB is taken as an example of evaluation. Nonetheless, as long as the current ripples in other systems are the same as those in the CHB, once the CHB is identified to be harmful or not for batteries, this conclusion will also be applicable for these systems.

With the objective of research defined, the rest of the article is organized as follows: In Section II, previous investigations on the influence of current ripples in the CHB are summarized, which proves the necessity of conducting an experimental investigation. Subsequently, the configurations of the experiment are introduced in Section III. Section IV, the results of the experiment are stated and explained, followed by a more general analysis trying to align different conclusions in previous studies. The applicability of cascaded multilevel topologies (with the same ripple patterns as in Fig. 2) in EVs is examined based on the aligned theory. In the end, a conclusion regarding the influence of current ripples is drawn based on the experimental results and discussions.

II. State-of-the-Art

In previous studies, current ripples in cascaded multilevel topologies with single-phase submodules, which are represented by the CHB in this article, are mostly deemed as harmful to lithium batteries. This can be partially proven by the availability of literatures focusing on the suppression of the current ripples in single-phase systems [31]–[40]. The studies regarding ripple suppression mostly do not directly verify that current ripples can damage batteries, but claim the damages in the introduction part by quoting the assertions in other studies. However, tracing back to the most original sources quoted in [31]–[40], only [41]–[44] are found to have conducted experiments with ripple current. Furthermore, in [41]–[43], the ripple current is implemented on lead-acid batteries or fuel cells. Hence, the obtained results are not applicable for the cascaded multilevel topologies using lithium batteries. Bala *et al.* [44] tested lithium battery cells with the current waveform shown in Fig. 2. The experiment in [44] measures the electrochemical efficiency and the temperature of the cells, when the cells are tested by current ripples. The results indicate that the differences caused by ripples are rather minimal. No long-term test is conducted to investigate the influences of the ripples on the battery aging. Therefore, the damages of the ripple current to lithium batteries claimed in [31]–[40] are not concretely supported by experimental results.

If not restricting the shape of the current ripples to be the same as the ripples in the CHB, shown in Fig. 2, a few more studies are found to have investigated the influence of ripple current in long-term battery aging experiments [45]–[49]. The ripple current waveforms in these studies are formed by superimposing a square or sinusoidal ripple current onto a constant dc current.

Uno and Tanaka [45] test 2 Ah lithium cobalt oxide (LiCoO2) cells with square wave current in float charging state. The square

waves have an amplitude of ± 1 A and the frequency of the waveforms varies from 1 to 10 kHz. In the experiment that lasted 147 days, if the frequency of the current waveform is 100 Hz or higher, the ripples show no impact on the battery aging. For cells tested by ripples with a frequency of 10 Hz or even lower, an additional capacity fade of about 7% is observed. Therefore, Uno and Tanaka [45] conclude that ripples in cascaded multilevel topologies are significantly harmful to the batteries, when the frequency is lower than a corner value. In the case of [45], the corner frequency is 10 Hz.

Kim *et al.* [46] investigate the influence of 120 Hz half sinewave ripples [46]. In each cycle, the tested cells are charged by the ripple current until the SOC is 80%, and discharged by constant dc current until the SOC equals 30%. After 250 test cycles, compared to the cells only tested by the constant dc current, the capacity reductions of the cells charged by ripple current are on average 0.55% higher. However, as the difference is low, the study does not confirm any concrete impact of the current ripples.

An aging test is conducted in [47] using the same ripple current waveform as in [46]. In each cycle, lithium battery cells are charged by ripple current, and then discharged on a resistor until 2.8 V. After 2000 cycles, the capacity losses of the dc-charged cell and the ripple-charged cell are, respectively, 15.1% and 16.3%. An additional capacity loss of 1.2% is attributed to the ripple current. However, [47] deems this magnitude of additional capacity loss as acceptable.

Breucker *et al.* [48] test the influence of switching frequency ripples in a dc/dc converter [48]. Using two different filter configurations, two 8 kHz ripple waveforms with different amplitudes 37.5 and 1 A, respectively, are generated. The two current waveforms are applied on two 40 Ah battery packs. A slightly higher capacity loss is observed on the pack tested by the higher ripples. Nonetheless, Breucker *et al*. [48] conclude the difference is not directly caused by the ripples, but by the increased cell temperature, which could have been eliminated with an improved cooling. Breucker *et al.* [48] explain the conclusion with the intrinsic equivalent double-layer capacitors of the batteries, which can effectively filter the switching frequency ripples.

The most recent result regarding the influence of ripples is published by Brand *et al*. [49]. Nickel manganese cobalt oxide (NMC) cells are tested, and the waveforms of the ripple current are generated by superimposing a sinusoidal current of ± 0.2 C onto a 0.225 C dc current. In the experiment, an additional capacity loss is observed on the cells tested by ripples. However, the difference is within 1%. The difference starts to appear after the first 50 cycles, and does not increase further as the test goes on. Therefore, it is suggested that the battery cells can tolerate the current ripples. Besides the direct experimental investigations, [49] also systematically summarizes and compares the results in previous studies, especially the experimental results in [45]. Brand *et al.* [49] reveal that the battery aging is not significantly influenced by ripples, as long as the temperature is kept the same as that of the cells tested by dc current. The contradictions with [45] are mainly explained by the difference in the method of cell capacity measurement.

In the earlier discussion, it is observed that the conclusions of existing studies are inconsistent. Brand *et al.* [49] indicate that the inconsistency of conclusions is caused by the difference in thermal management and measurement methods, and that current ripples are not harmful to batteries. Nonetheless, due to the differences between the ripple waveform in [49] and the ripple waveform in the CHB, the conclusions in [49] are not directly applicable for the batteries in the CHB.

First, compared to the sinusoidal ripples with a single frequency in [49], the ripple current in the CHB is a compound of multiple frequencies, as visible in Fig. 2. An additional compound effect of different frequencies is possible. Second, the peak C-rate of the current ripples in the CHB is much higher than those in [45]–[49]. It cannot be directly confirmed if the conclusion in [49] still holds, when the amplitude of the ripples becomes much higher. Third, the most significant difference is that the battery current in the CHB crosses zero frequently, and hence forms a large amount of microcycles. Similar microcycles do not exist in the waveforms of the previous studies, except for [45]. That means the ripples in [46]–[49] do not change the charge throughput. In the analysis of [49], however, this factor is only briefly mentioned in the discussion and not explicitly investigated.

Additionally, for the investigation on the ripple current in the CHB, battery aging models [27]–[30] are not capable of generating a concrete conclusion, due to the limit of the time resolution and modeling approach. Furthermore, in an aging simulation, the conventional equivalent circuit model of battery cells [50] is often used to provide inputs to the cell aging models. However, according to the experimental results in [45] and [49], the equivalent circuit model tends to neglect the filtering effect of the battery cells and significantly overestimate the aging caused by current ripples.

As previous studies cannot provide a concrete conclusion whether current ripples are harmful to batteries or not, and a dedicated investigation is not possible to be conducted in simulations, an experimental investigation is necessary. In the experiment, the current ripples in the CHB is taken as the representative of the current ripples in cascaded multilevel topologies that have single-phase submodules. The long-term influence on the aging of batteries is monitored. Hence, a concrete conclusion regarding the influence of current ripples can be drawn accordingly.

III. Aging Experiment

In this section, the hardware to generate ripple current and the configurations of the experiment are introduced. In order to examine the influence of current ripples in the CHB, five battery cells are cycled with different current waveforms until their end of life. Different ripple current waveforms are generated by varying the power factor and the switching frequency of the CHB.

A. Design of the Test Rig

For the experimental investigation, a specific test rig is designed to generate the high frequency current ripples. Nonetheless, to generate the battery current waveform in a CHB, this article does not put cells directly in H-bridges and discharge

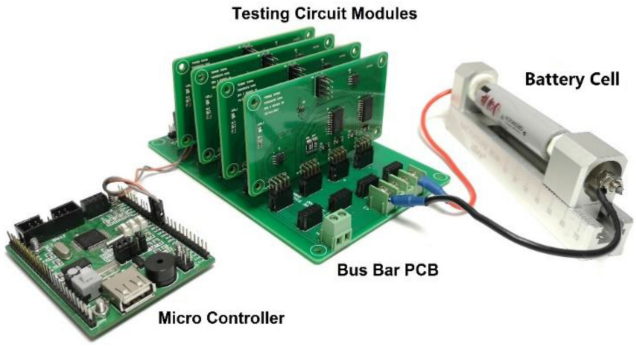

Fig. 3. The test rig for one battery cell.

TABLE I
PARAMETERS OF THE RIPPLES CURRENT WAVEFORMS TO DISCHARGE THE CELLS

Cell No.	Parameters of the current waveform to test each cell					
	DC or not	Switch freq.	Power factor	AC freq.	Ave. C-rate	RMS C-rate
Cell 1	Yes	-	-	-	0.8 C	0.8 C
Cell 2	Yes	-	-	-	0.8 C	0.8 C
Cell 3	No	2 kHz	0.8	100 Hz	0.8 C	1.32 C
Cell 4	No	10 kHz	0.8	100 Hz	0.8 C	1.32 C
Cell 5	No	10 kHz	0.9	100 Hz	0.8 C	1.22 C

to a load resistor. On the one hand, if H-bridges are directly used to create the current ripples, the accuracy of the current will be influenced by the accuracy of the load resistors and inductors. Tuning the accuracy of the current waveforms will be consequently more inconvenient and time-consuming. On the other hand, if conducting the cycling test of the cells in H-bridges, an additional power supply will be required by each H-bridge to charge the tested cell, which tends to make the experimental setup more complicated.

Therefore, as an alternative solution, this article uses power analog circuits to generate the required current waveforms. The accuracy of the current can thus be ensured by simply selecting components with high open-loop gains in a wide range of frequency and temperature. With the selection of components in this design, especially the selection of operational amplifiers and high speed digital to analog converter, a bandwidth of 0 to 400 kHz is realized, which is sufficient to ensure the current accuracy of the experiments. Additionally, since the designed power analog circuits have bidirectional output capability, the cells can be both charged and discharged in the test rig. An assembled test rig is shown in Fig. 3. The vertically inserted boards are the power analog circuit modules. They are paralleled by the bus bar printed circuit board (PCB) underneath to enhance the maximum output capability.

Before the experiment, the output current waveforms of all the test rigs are measured by the current probe HZO51 and the oscilloscope HMO724 from Rohde and Schwarz. The accuracy of the current waveforms is proven to be within a few percent. Hence, the experiment results are not expected to be distorted by the inaccuracy of the waveforms. Further, an electronic load, Agilent N3300A, which provides an accuracy of 0.1% for voltage and current according to the manual, is used for the measurement of cell capacity and inner resistance. As the test rig design is not relevant to the main topic of this article, the details of the circuit is not further introduced.

B. Configuration of the Experiment

In the aging experiment, five Panasonic NCR18650BD cells are cycled until their end of life. The cells have a nominal capacity of 3 Ah. The cathode material of these cells is NMC and the gravimetric energy density is 217 Wh/kg. According to the datasheet [51], the full cycle life of the cell is only 500. That means after 500 charge/discharge cycles, with a cycle depth of 100% (corresponding to cycling between 4.15 and 2.5 V), the cells are expected to lose 20% of their original capacity. The five cells are numbered and tested by different ripple current waveforms that are generated by the test rigs shown in Fig. 3. Cells are put in the open air of the laboratory, which has a stable temperature of 21 °C due to the air conditioning setting. The parameters of the current waveform for each cell are given in Table I. The waveforms in Table I are only used for the discharge. All five cells are still charged by dc current in the aging test.

All the five current waveforms for discharging have the same average C-rate, 0.8 C, in case that the difference in average C-rate could potentially distort the results. This C-rate is determined by the maximum C-rate encountered in common driving cycles. The average values of all five current waveforms are 2.4 A. Among the five cells, cells 1 and 2 are tested by the dc current as the control group. The other three cells, cell 3–5, are tested by different ripple current waveforms and form the experimental group.

The ripple current waveforms are described by the working conditions of the CHB, where the corresponding current ripples can be observed, as given in Table I. The three ripple current waveforms are differentiated from each other by the switching frequency and the power factor of the CHB. To demonstrate the current waveforms in a clearer manner, the measured current waveforms to test cell 3–5 are depicted in Fig. 4. Comparing cells 3 and 4, the switching frequency of is varied, but the amplitude of the ripples and the depth of the microcycles stay constant. Hence, comparing the aging behaviors of cells 3 and 4, the influence of high frequency ripples could potentially be identified.

The current waveform of cell 5 is differentiated from that of cell 4 by the power factor, $\cos\theta$. If $\cos\theta$ decreases (phase lag increases), the negative part of the waveform will expand, because the zero-crossing point of the ac voltage moves further to the left and the current is flipped to negative earlier. Consequently, the depth of the microcycles increases. In order to maintain the average C-rate at 0.8 C and compensate for the increased negative current, the peak value of the current should also be increased. Therefore, as $\cos\theta$ decreases, the peak value of the current and the depth of microcycles increase accordingly, which could deteriorate the battery aging. Cos θ defines the

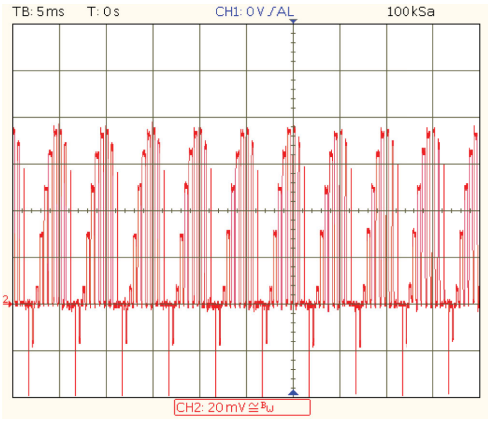

(a)

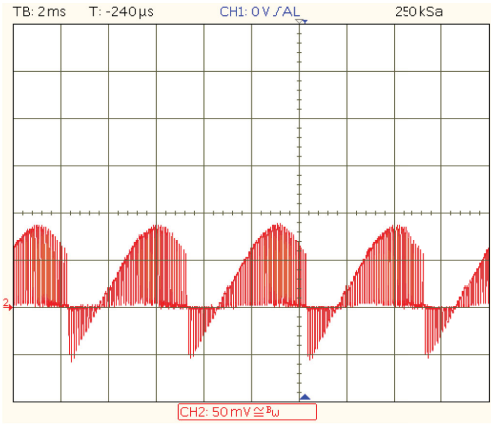

(b)

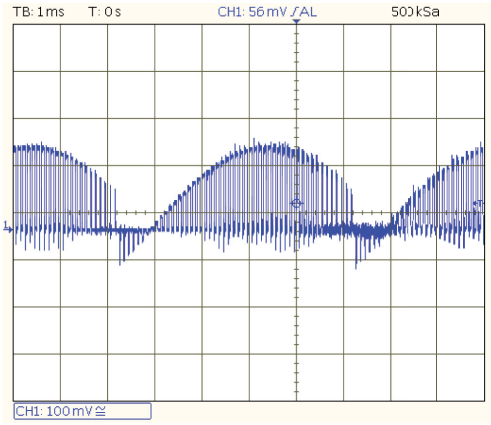

(c)

Fig. 4. Measured current waveform for cells 3, 4, and 5. (a) Current waveform of cell 3, 10 mV/A. (b) Current waveform of cell 4, 10 mV/A. (c) Current waveform of cell 5, 20 mV/A.

amplitude of each pulse and the depth of the microcycles in the current waveforms. Comparing cells 4 and 5, the influence of the power factor can be investigated.

Additionally, all three ripple current waveforms are generated implying that the CHB is working with a modulation index of 0.8. That means each cell is equivalently supplying an ac voltage with a peak value of $0.8u_{\mathrm{bat}}$ to the load. u_{bat} is the voltage of the battery cell. With the modulation index given,

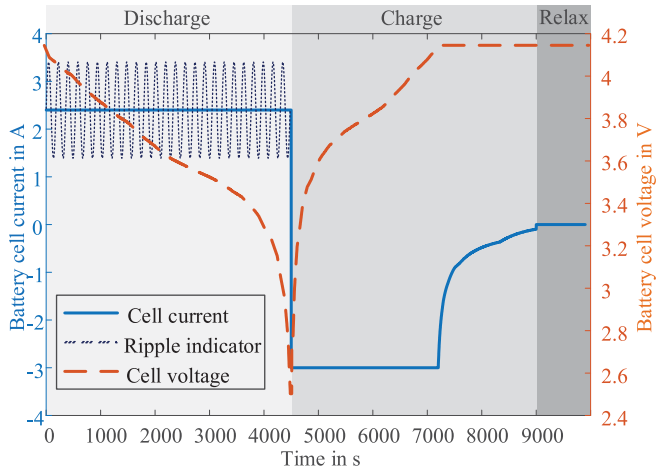

Fig. 5. Test profile of the aging experiment.

the duration of each pulse in the current waveforms can be determined accordingly.

After introducing the discharging current waveforms, the current and voltage profile of one test cycle is demonstrated in Fig. 5. The profile is applicable for all the cells, regardless of the discharge waveform settings. As visible in the voltage curve (the dotted curve, corresponding to the right *Y*-axis), every test cycle starts from a cell voltage of 4.15 V. The cells are first discharged by the corresponding 0.8 C current waveforms in Table I, marked by the ripple indicator and the current curve (solid curve, corresponding to the left *Y*-axis). A positive current value refers to discharge. The discharge continues until the terminal voltage of the battery reaches 2.5 V, and the charge immediately starts.

The charge of all the battery cells follows the common constant current constant voltage (CC-CV) scheme. No ripple is injected during the charging process of all cells. The charge starts with 3 A CC charging (1 C charging) and switches to CV charging, once the terminal voltage reaches 4.15 V. When the charge current is lower than 100 mA, the charging process stops. In the end, after the cells are fully charged, a relaxation time of 15 min is provided to the cells, before entering the next testing cycle. The cycle depth of this testing profile is thus 100%. One cycle for a brand new cell takes almost three hours.

After every 50 cycles, the cells are taken out from the testing rigs to measure their capacity (1 C discharge capacity) and inner resistance (200 ms dc resistance at 80% SOC) manually. The cells are measured by discharging to the electronic load introduced in the previous section. Including the measurements, the 500 cycles took more than three months, started from September of 2017, ended in January of 2018. The results of the aging experiment are discussed in Section IV.

IV. Results

In this article, the inner resistance and the capacity of the cells are recorded, in order to monitor the aging behaviors of the cells tested by different current waveforms. In this section, the measured capacity reductions and the resistance increases of

TABLE II
CAPACITY OF THE CELLS MEASURED OVER THE WHOLE AGING EXPERIMENT

Number of cycles	The capacity normalized according to the initial capacity of each cell				
	Cell 1	Cell 2	Cell 3	Cell 4	Cell 5
0	100 %	100 %	100 %	100 %	100 %
50	92.7 %	92.6 %	92.4 %	92.2 %	92.5 %
100	89.7 %	89.5 %	89.2 %	88.9 %	89.4 %
150	84.3 %	83.3 %	85.7 %	85.5 %	83.9 %
200	88.3 %	87.4 %	88.3 %	85.4 %	86.8 %
250	86.2 %	85.9 %	86.3 %	82.8 %	85.0 %
300	84.4 %	84.8 %	86.3 %	81.8 %	84.4 %
350	85.1 %	82.7 %	83.7 %	80.4 %	83.2 %
400	82.9 %	81.9 %	82.4 %	80.6 %	81.7 %
450	82.5 %	82.6 %	81.6 %	78.9 %	80.2 %
500	79.8 %	80.2 %	78.6 %	77.5 %	77.6 %

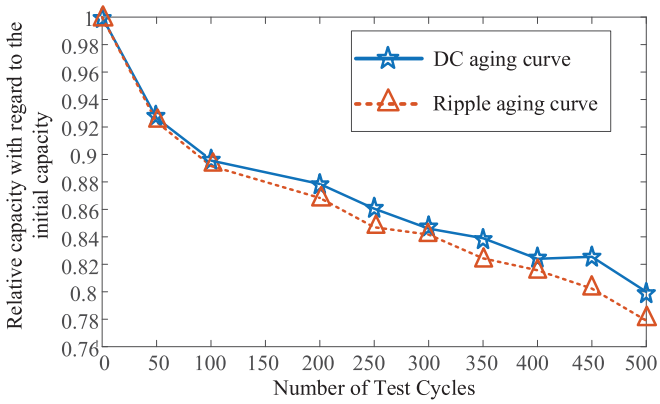

Fig. 6. Average capacity reduction curves of the cells tested by dc current and ripple current.

the five cells are introduced in Section IV-A. Then, in Section IV-B interprets the indications of the experimental results, in order to conclude if current ripples in the CHB are harmful for batteries.

A. Results of Measurement

The measured capacity reductions of the five cells are given in Table II. With the results obtained in Table II, the average capacity reduction curves of the dc-tested cells and the ripple-tested cells are plotted in Fig. 6.

In Fig. 6, the solid curve depicts the average capacity reduction of the two cells tested by the dc current, i.e., cells 1 and 2. The dotted curve depicts the average capacity reduction of cells 3–5, which are tested by current ripples. As illustrated in Fig. 6, in the first 100 cycles, there is no visible difference between the cells tested by dc current and ripple current. Nonetheless, since the 200th cycle, a small difference around 2% is established. From then on, the average capacity loss of the ripple-tested cells is

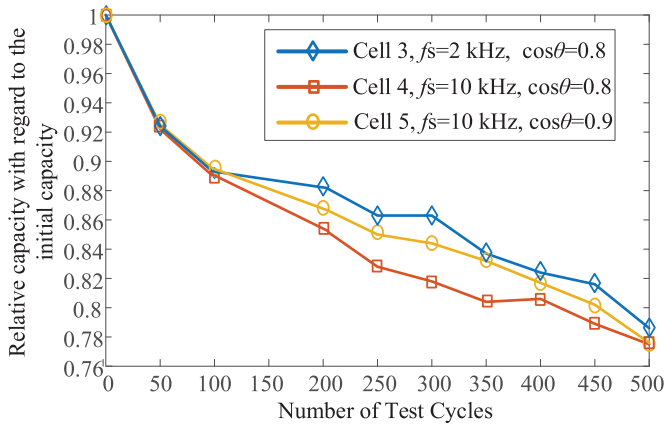

Fig. 7. Three aging curves of the cells tested by ripple current waveforms.

constantly around 2% higher than that of the dc-tested cells. At the end of the experiment, the dc-tested cells still have a capacity of 80.0% on average, while the average residual capacity of the ripple-tested cells is 77.9%. In the end of the experiment, the ripple current is identified to cause an additional capacity loss of 2.1% on average.

To investigate the influence of the power factor and the switching frequency, the aging curves of cells 3–5 are also compared to each other in Fig. 7. In the first 100 cycles, almost no difference can be identified between the three curves. The difference starts to appear from the 200th cycle. From the 200th cycle, the residual capacities of cells 3 and 5 are constantly higher than that of cell 4. However, from the 400th cycle until the end, the difference of the three curves rapidly converges. Cells 3–5 even have almost the same residual capacity in the end. Therefore, at the end of life, the difference in switching frequency or the difference in power factor does not cause any difference in terms of capacity reduction.

The divergence of the capacity curves from the 200th to the 400th cycle could be explained by the stochastic property of the aging, because the residual capacity values of the three cells are close to each other in the end of the experiment. Similar phenomena and explanations are reported in previous studies as well [52]–[55]. Comparing the capacity reductions of cells 1 and 2 in Table II, which are tested by dc current, a divergence with a similar magnitude is also observed from the 250th to the 450th cycle. Therefore, the capacity divergence in the aging test is further confirmed not specific to the parameters of current ripples.

Besides the capacity reduction curves, the records of the inner resistance are also analyzed. The aging curves of the 200 ms dc resistance of the cells are plotted in Fig. 8. After 500 cycles of aging test, the inner resistance of all the cells is increased from 50–60 mΩ to 90–100 mΩ. However, the resistance values of the five cells are rather close to each other over the whole experiment. The five cells cannot be differentiated from each other by the difference in resistance growth. The spread of the resistance values does not change much after 500 cycles of aging test as well. The maximum difference of the inner resistance only grows from 8 to 10 mΩ.

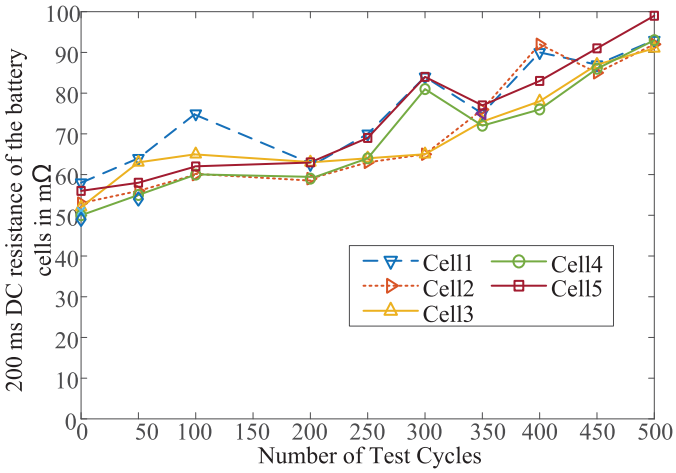

Fig. 8. 200-ms dc resistance of the cells measured over the entire aging test.

In the end, it is worth noting that the measurement results at 150th cycle are not plotted in Figs. 6, 7, or 8, because the batteries were not fully charged in the capacity measurement due to an operation error, and the measurement values were significantly lower. This operation error was only discovered, when the capacity values at 200th cycle were obtained and show a significant capacity recovery. Hence, it is not possible to redo the measurement at 150th cycle. However, as the experiment had taken long time by then, and the removal of one point does not influence the validity of the experiment or the final conclusion, the experiment was continued.

In this section, the experimental results are introduced. The ripples seem to have negative influence on the capacity loss, while the increase of inner resistance seems not influenced at all. In order to determine if the CHB or other cascaded multilevel topologies with the same ripple patterns should be rejected for BESSs due to the additional capacity loss, the following section further analyzes the results and the potential influence on the system level.

B. Interpretation of the Results

The aging experiment shows that the current ripples in the CHB increased the capacity reduction of battery cells by 2.1%. Compared to the end-of-life criterion, 20% loss of the original capacity, the ripples have accelerated the aging by 10%, which seems to be significant. However, on the system level, this additional capacity loss can be neglected, which makes the CHB or other cascaded multilevel converters with the same ripple pattern still an attractive concept.

First, although the capacity on cell level is reduced by the current ripples, the usable capacity on the pack level will not be influenced to the same extent, because the CHB can actively balance the SOC of battery modules via different PWM algorithms [56], [57], instead of dissipating the energy on the battery management system. Due to the balancing capability, when using the same cells, the CHB or cascaded multilevel topologies with the same ripple patterns have a higher capacity on the pack level than a conventional battery pack. Consequently, the additional capacity loss on the cell level can be counterbalanced on the pack level. The extent of the counterbalance is determined by the spread of the cell capacities. For aged cells or large cells, which have a capacity spread of above 4% potentially to be balanced by cascaded multilevel topologies [58], [59], the additional capacity loss of 2.1% could be fully counterbalanced. Therefore, for cascaded multilevel topologies with the same ripple patterns, only when the additional capacity loss is much higher than the capacity spread, the additional capacity loss can be considered significant.

Second, due to the limited number of samples in the experiment and the stochastic property of the aging, the observed additional capacity loss might be overestimated. In the experiment of [49], where 20 cells were tested and a similar behavior of capacity aging was observed (referring to the fact that a small additional capacity loss also appears in the first 100 cycles and does not further increase in [49]), the additional capacity loss attributed to current ripples is below 1%. This value could be a better estimation of the average influence of ripples than the results of this article, and hence indicates that the negative influence of the ripples could be overestimated by the experiment in this article.

Third, in Fig. 8, it is seen that the degradation of the inner resistance is not influenced by the current ripples. Therefore, in terms of the efficiency and the maximum power, which are determined by the inner resistance, the performance of the cells is not deteriorated by the current ripples. The usable capacity measured at the output of the cells is thus not influenced.

To summarize, although the CHB or other cascaded multilevel topologies with the same ripple patterns could cause a small additional capacity loss, this additional capacity loss can be counterbalanced by the active balancing capability on the pack level. The degradation of the inner resistance is not influenced and thus does not limit the usable capacity of the cells. Consequently, the influence of current ripples on the aging can be determined as insignificant. The cascaded multilevel topologies remain an attractive concept.

V. Discussion

According to the results in Section IV, the current ripples in the CHB have no significant influence on the aging of batteries. In this section, the insignificance in the experiment is explained. Subsequently, the contradiction with the observations in [45] is discussed. Based on the discussion, the preconditions for ripples to become harmful can be identified. In the end, the applicability of the CHB is examined for EVs.

A. Explanation of the Insignificant Influence

Compared to the experiments in [46]–[49], although the ripples in the CHB or other cascaded multilevel topologies with the same ripple patterns have a much higher ripple component, the conclusions of experiments are similar. The similarity of the results can be mainly explained by the heat increase and the total charge throughput of the cells, which are the two factors that ripples could possibly influence the aging behaviors [49].

First, with the same cooling, the temperature increase caused by ripples is only linked to the rms value the ripples, because the heat in the cells is generated by the ohmic losses on the inner resistance. The rms value of the battery current in the CHB, $I_{\mathrm{bat\_RMS}}$, can be calculated using (1). T_{s} is the time length of one switching period. I_{ACpeak} is the peak value of the phase current. m_{a} is the modulation index. θ is the phase lag between the phase current and the phase voltage. N is the carrier index. Assuming N approaches to infinite, the sum in (1) can be further converted to an integral and gives an analytical. $I_{\mathrm{bat\_ave}}$ is the average value of the battery current. With the rms value of the battery current obtained, the rms value of the ripple component, $I_{\mathrm{ripple\_RMS}}$, is determined by (2)

$$\begin{aligned} &I_{\mathrm{bat\_RMS}} \\ &= \sqrt{\frac{1}{N}\sum_{k=1}^{N}\left[I_{\mathrm{ACpeak}}\sin\left(\frac{k\pi}{N}-\theta\right)\right]^2\cdot m_a\sin\frac{k\pi}{N}\cdot T_{\mathrm{S}}} \\ &= \sqrt{\frac{m_a I_{\mathrm{ACpeak}}^2}{\pi}\int_0^{\pi}\sin\omega t\sin^2(\omega t-\theta)d\omega t} \\ &= \frac{2I_{\mathrm{bat\_ave}}}{\cos\theta}\sqrt{\frac{(1+\frac{1}{3}\cos 2\theta)}{\pi m_{\mathrm{a}}}} \end{aligned} \tag{1}$$

$$I_{\mathrm{ripple\_RMS}} = \sqrt{I_{\mathrm{bat\_RMS}}^2 - I_{\mathrm{bat\_ave}}^2}. \tag{2}$$

Substituting the experimental settings into (1) and (2), i.e., cos θ and m_{a} are both 0.8, the value of $I_{\mathrm{bat\_RMS}}$ equals $1.64I_{\mathrm{bat\_ave}}$. That means the rms value of the ripples is 64% of the dc current. Changing cos θ to 0.9, the percentage value becomes 53%. Therefore, the rms values of the ripples in the CHB are, in fact, comparable to those in [46]–[49]. Hence, a similar temperature increase is expected in cells. The peak C-rate of the ripples is indeed much higher, but the rms values are relatively low and only cause a limited temperature increase.

On the other hand, the influence of a higher rms caused by the CHB can be quantitatively estimated by based on the heat generation and the temperature measurements of a previous study [60]. First, in the worst case, assuming the ripple current flows through the same resistance as the dc current does (which is not the case), heat generations of cells 3–5 are, respectively, increased by 167%, 167%, and 134% by the higher rms values. Second, according to the measurement results in [60], when passively cooled, 1C discharge on a 18 650 cell results in a temperature increase of 6 °C compared to the ambience while 2C discharge (corresponding to a 300% heat generation increase) realizes an increase of 11 °C. A simple linear interpolation between the two points thus estimates the additional temperature increases caused by the ripples on cells 3–5 to be, respectively, 2.8 °C, 2.8 °C, and 2.2 °C, when the average discharge rate is 1C. It is seen that the additional temperature increase caused by the ripples is insignificant even in the worst case. And according to the aging model in [30], these worst case additional temperature increases correspond to an extra capacity loss of lower than 0.5% during the test. Therefore, the insignificant thermal influence of the ripples in the CHB can also be quantitatively confirmed.

TABLE III
RMS VALUES AND CHARGE THROUGHPUT OF THE CURRENT WAVEFORMS USED TO TEST THE FIVE CELLS

Cell No.	Calculated parameters of the current waveforms					
	DC or not	cosθ	$I_{\mathrm{bat\_ave}}$	$I_{\mathrm{bat\_RMS}}$	$I_{\mathrm{ripple\_RMS}}$	$I_{\mathrm{Q\_MCycle}}$
Cell 1	Yes	-	2.4 A	2.4 A	0	0
Cell 2	Yes	-	2.4 A	2.4 A	0	0
Cell 3	No	0.8	2.4 A	3.95 A	3.14 A	0.16 C/s
Cell 4	No	0.8	2.4 A	3.95 A	3.14 A	0.16 C/s
Cell 5	No	0.9	2.4 A	3.67 A	2.78 A	0.05 C/s

Besides the rms value of the current, the charge throughput of the batteries in the CHB is also assessed to evaluate the influence of the microcycles. In [46]–[49], as the battery current never crosses zero, the charge throughput of the ripple-tested cells is expected to be the same as the throughput of dc-tested cells. However, for the CHB, due to the microcycles, the charge throughput of the cells is increased. The rate of the additional charge throughput caused by microcycles, $I_{\mathrm{Q\_Mcycle}}$, is defined in (3). Following the same approximation approach as in (1), an analytical solution of $I_{\mathrm{Q\_Mcycle}}$ is provided in (3). T_{AC} is the period of ac voltage

$$I_{\mathrm{Q\_Mcycle}} = \frac{\int_0^{T_{\mathrm{AC}}}|i_{\mathrm{bat}}|}{T_{\mathrm{AC}}} - I_{\mathrm{bat\_ave}} = \frac{2I_{\mathrm{bat\_ave}}}{\pi}(\tan\theta-\theta). \tag{3}$$

The charge throughput of microcycles is only influenced by the power factor of the CHB, cos θ. When cos θ is 0.8 or 0.9, $I_{\mathrm{Q\_Mcycle}}$ equals respectively $0.069I_{\mathrm{bat\_ave}}$ or $0.021I_{\mathrm{bat\_ave}}$. That means that the microcycles increase the charge throughput of the cells correspondingly by 6.9% or 2.1%. This extent of increase is insignificant, as the aging is not linear with the charge throughput. According to the aging model in [30], even if assuming all the extra charge throughput effectively contributes to the aging, the additional capacity loss is estimated to be 0.33%. Besides, as proven in [45] and [49], a large amount of throughput can actually be filtered and results in an even lower capacity loss.

Due to the similarities in terms of the temperature increase and the charge throughput, the similarities of the results in this paper to those in [46]–[49] can be explained. The rms values and the microcycle throughputs of the five cells discussed above are in Table III for the convenience of cross checking. The absolute values are given, but they can be converted to C-rate by dividing them with the nominal capacity, 3 Ah. Unit C/s refers to Coulombs per second, as the microcycles are not directly measurable current.

B. Explanation of the Contradiction and the Formation of an Aligned Theory

Uno and Tanaka [45] implemented microcycles in the aging test of lithium batteries, however, the obtained conclusion is contradicting the conclusion of the experiment in this article. Therefore, in the second part of the discussion, the contradiction to [45] is explained by analyzing the stress factors caused by the

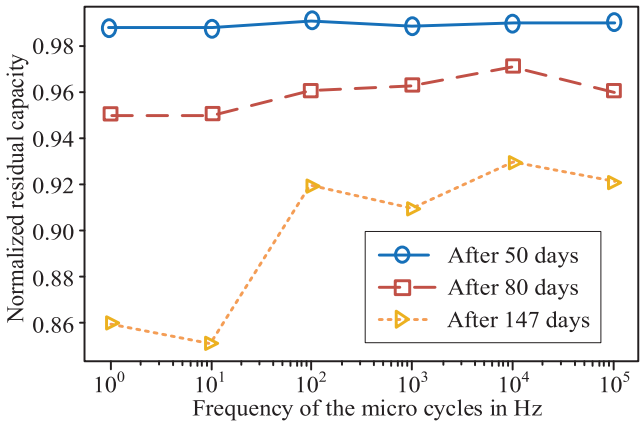

Fig. 9. Capacity reduction observed in the aging experiment of [45], with and without current ripples.

current ripples. Further, by explaining the contradiction with [45], an aligned theory regarding the influence of ripple current can be established.

In [45], all the cells are working in float charging status and tested by ripples at different frequencies. The results are shown in Fig. 9. The three curves are obtained respectively after 50, 80, and 147 days of continuous tests. At the end of the experiment, the cells that are tested by low frequency ripples experience an additional capacity loss of 7%, almost twice the capacity loss observed on the other cells. The capacity loss of the cells tested by high frequency ripples shows no difference. Therefore, Uno and Tanaka [45] conclude that current ripples are significantly harmful for batteries, if the frequency is lower than 10 Hz.

Such an accelerated aging caused by low frequency ripples is not visible in other studies or in this article. Brand *et al.* [49] suggest this contradiction is mainly because of the method for capacity measurement. However, by analyzing the test configurations of [45], the significant difference can be better explained by the amplified effect of the charge throughput caused by the ripples.

In [45], the cells are working in float-charging state. The current injected to the cells only contains microcycles (± 1 A square waves). Average values of the current waveforms are zero. Hence, in [45], the charge throughput of the cells is only caused by the microcycles. For the 2 Ah NMC cells in [45], after 147 days of test, the accumulated charge throughput of each cell is equivalent to 882 full cycles. In comparison, for the CHB, even if the power factor is 0.8, after 500 cycles of test, the charge throughput caused by microcycles is only equivalent to 17 full cycles. Consequently, in the case of [45], the filtering effect of the battery for different frequencies becomes the most determining factor for the aging of batteries.

For microcycles at higher frequencies, because the large amount of additional charge throughput can be removed completely, no extra aging is observed. That explains the consistency of the ripples at 100 Hz or a higher frequency. For the microcycles below 10 Hz, because the throughput can only be partially filtered, a significant impact on the aging is expected, which explains the 7% extra capacity loss. In fact, according to the aging model in [30], the 7% extra capacity loss corresponds to 180 additional effective full cycles. That means around 80% of the throughput at the terminal is still removed by the filtering effect.

Based on the analysis above, it is seen that the conclusion in [45] is also reasonable. The conclusion reveals the influence of the current ripples in a certain scenario, where the cells are not cycled but only exposed to microcycles. In [46]–[49] and the experiment of this article; however, the impact of microcycles is restricted.

After confirming the negative conclusion in [45] regarding the ripples is also reasonable, by summarizing the discussions earlier, three preconditions for a ripple current waveform to be harmful can be summarized as follows.

1) The ripples result in microcycles or high rms values.
2) The frequency of microcycles is lower than 10 Hz or a corner frequency determined by experiments.
3) Microcycles form a large total charge throughput or high rms values create a significant temperature increase.

First, the ripples should contain microcycles or result in a significant increase of the rms value. Otherwise, as long as a sufficient cooling power is provided to the cells, the ripples are expected to have no impact on the aging, because the temperature increase of the cells can be well restricted. Second, the microcycles must have a frequency lower than 10 Hz. Third, the working state of the batteries should allow microcycles to contribute a large amount of charge throughput, or allow the increased rms value of the ripples to create a high temperature increase. An example where three preconditions are all met is float charging. In this case, the extra charge throughput caused by the microcycles can effectively cause extra degradations to the battery cells.

The three preconditions can be used to examine if the current ripples in a certain system or in a certain scenario are harmful to batteries. An example of such an examination is provided in the following section, where the applicability of the CHB or other cascaded multilevel topologies with the same ripple patterns in EVs is discussed.

C. Applicability of Cascaded Multilevel Topologies in EVs

Based on the three preconditions obtained in the final section, this section examines the applicability of the CHB and cascaded multilevel topologies with the same ripple patterns in EVs. A number of studies proposed to use cascaded multilevel topologies for EVs due to different motivations [14], [61]–[63]. These proposals should be reconsidered, if the current ripples significantly accelerate the aging.

In the CHB, when the vehicle is driving at a low speed, the frequency of the microcycles is possible to be lower than 10 Hz. However, specifically for EVs, the possibility of this situation is extremely low.

First, to make the frequency of microcycles below 10 Hz, the ac frequency of the powertrain system must be lower than 5 Hz. Nonetheless, as automotive motors usually have a nominal frequency of 200 Hz or above [64]–[66], such a low frequency corresponds to an extremely low speed of the vehicle. Hence,

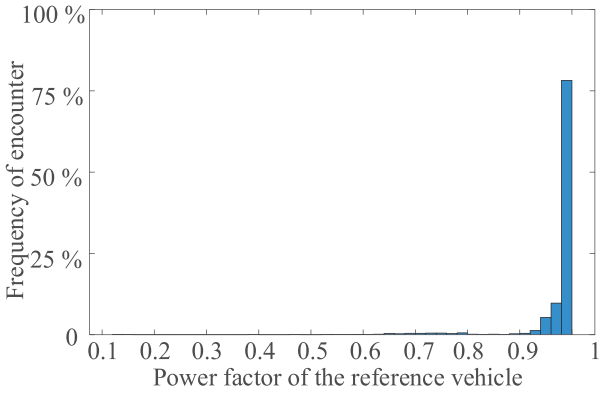

Fig. 10. Histogram of power factor values in the reference vehicle, when tested by WLTP C3 driving cycle.

this situation can rarely be encountered in a realistic driving scenario. According to the powertrain model developed in [14], for a typical EV model, BMW i3, an ac base frequency of 5 Hz corresponds to a vehicle speed of only 0.8 km/h. The possibility to meet the precondition regarding the frequency is negligible.

Second, in an EV, the additional charge throughput caused by the CHB is limited, because the power factor of the motors in EVs is usually high. For vehicles equipped with a permanent magnet synchronous motor (PMSM), the power factor is almost constantly close to 1.0. Still using the powertrain model in [14] of a BMW i3, which is driven by a PMSM, the vehicle is simulated in the WLTP C3 driving cycle. The distribution of the power factor is plotted in the histogram in Fig. 10.

It is seen that the power factor is almost constantly above 0.9, when the vehicle is following the WLTP C3 driving cycle. Considering the filtering effect of batteries, the effective charge throughput caused by microcycles is negligible.

For an EV driven by an induction motor (IM), the power factor is relatively lower, but still constantly above 0.65 [64], [67]. The corresponding increase in the charge throughput at the terminals of cells is thus 20% in the worst case, according to (3). However, according to the results in [45], for microcycles at 10 Hz or lower frequencies, the filter effect is still able to remove 80% of the additional charge throughput. Therefore, even if the IM would be constantly operating at a power factor of 0.65 and with a frequency under 5 Hz, the effective increase in the charge throughput would still be limited to 4%, corresponding to an additional capacity fade below 1% [30]. As a result, even in the worst case, the influence of the CHB on the aging is still insignificant.

In summary, although the first and the second preconditions are possible to be met for cascaded multilevel topologies in EVs, the additional aging caused by the ripples is still expected to be negligible, because the third precondition, a significant charge throughput caused ripples, does not hold. Therefore, cascaded multilevel topologies can be concluded to be generally applicable for EVs.

This section only provides an example to use the three preconditions. For a BESS in different applications, in order to examine the applicability of cascaded multilevel topologies with the same ripple patterns as the CHB, a similar assessment can be conducted.

VI. Conclusion

A number of studies have proposed to use different cascaded multilevel topologies in stationary or on-board BESSs, due to the advantages [21]–[24], [61]–[63] in different aspects. As the batteries in these topologies only supply the power for a single phase, the battery current contains large ripples. However, so far no study has dedicatedly investigated whether the current ripples in these topologies could significantly accelerate the aging of batteries, which could fundamentally influence the applicability of these topologies in BESSs. Motivated by the gap of research, taking the CHB as a representative, this article investigates the influence of cascaded multilevel topologies that have the same ripple patterns as the CHB, via a long-term aging experiment and the analysis of the experiments in existing studies.

The experiment proves that the ripples in the CHB or other cascaded multilevel topologies with the same ripple patterns are not supposed to cause a significant damage on the batteries, regardless the switching frequency and the power factor. An additional capacity reduction is observed, but the difference is small and could be compensated by the SOC balancing capability. Similar insignificant influence is also observed in [68] and [69], where double ac frequency and switching frequency ripples were also used, although the tested current waveforms are different from those in the CHB.

The insignificant influence is further explained by the limited rms value of the ripples and the limited increase in charge throughput of cells. By analyzing the experimental configurations in [45], which draws a negative conclusion regarding the influence of the current ripples, three preconditions for the ripples to be harmful are identified, based on which an assessment process is recommended to evaluate the feasibility of cascaded multilevel topologies. The process is demonstrated on an electric powertrain, and cascaded multilevel topologies are confirmed generally applicable for the on-board BESSs of EVs.

However, this article does not indicate that all cascaded multilevel topologies are applicable for all BESSs. First, if the ripple patterns in a certain topology are different from those in the CHB, a dedicated investigation is still required. Second, in scenarios with a constantly high C-rate, due to the increasingly significant thermal influence, the conclusion might also not hold anymore. Further, if a BESS is constantly exposed to microcycles even in idling period, similar to the experimental configurations in [45], cascaded multilevel topologies should be avoided. One example of such a system is a charger for batteries working in float charging.

In the end, it is worth noting that the major limitation of the research is the limited number of cells in the experiment. Therefore, the experimental results in this article can only provide a directional conclusion that the influence of the ripples in the experiment is insignificant. The 2.1% additional capacity reduction observed in the experiment should not be taken as a strict quantitative result, due to the limited number of samples and the stochastic property of the battery aging behaviors. Additionally, the conclusion of this article is restricted to lithium batteries.

The conclusion and analysis in this paper are not applicable for systems using other energy storage methods, e.g., lead-acid batteries or fuel cells.

REFERENCES

[1] J. Cao and A. Emadi, "A new battery/ultracapacitor hybrid energy storage system for electric, hybrid, and plug-in hybrid electric vehicles," *IEEE Trans. Power Electron*., vol. 27, no. 1, pp. 122–132, Jan. 2012.

[2] S. Hu, Z. Liang, and X. He, "Ultracapacitor-battery hybrid energy storage system based on the asymmetric bidirectional z-source topology for EV," *IEEE Trans. Power Electron.*, vol. 31, no. 11, pp. 7489–7498, Nov. 2016.

[3] J. P. F. Trovao, M.-A. Roux, E. Menard, and M. R. Dubois, "Energy- and power-split management of dual energy storage system for a three-wheel electric vehicle," *IEEE Trans. Veh. Technol.*, vol. 66, no. 7, pp. 5540–5550, Jul. 2017.

[4] S. S. Williamson, A. K. Rathore, and F. Musavi, "Industrial electronics for electric transportation: current state-of-the-art and future challenges," *IEEE Trans. Ind. Electron.*, vol. 62, no. 5, pp. 3021–3032, May 2015.

[5] F. Liu, J. Liu, H. Zhang, and D. Xue, "Stability issues of Z + Z type cascade system in hybrid energy storage system (HESS)," *IEEE Trans. Power Electron*., vol. 29, no. 11, pp. 5846–5859, Nov. 2014.

[6] N. Mukherjee and D. Strickland, "Control of second-life hybrid battery energy storage system based on modular boost-multilevel buck converter," *IEEE Trans. Ind. Electron.*, vol. 62, no. 2, pp. 1034–1046, Feb. 2015.

[7] N. Tashakor, E. Farjah, and T. Ghanbari, "A bidirectional battery charger with modular integrated charge equalization circuit," *IEEE Trans. Power Electron.*, vol. 32, no. 3, pp. 2133–2145, Mar. 2017.

[8] N. Saxena, I. Hussain, B. Singh, and A. L. Vyas, "Implementation of a grid-integrated pv-battery system for residential and electrical vehicle applications," *IEEE Trans. Ind. Electron.*, vol. 65, no. 8, pp. 6592–6601, Aug. 2018.

[9] P. C. Loh, L. Zhang, and F. Gao, "Compact integrated energy systems for distributed generation," *IEEE Trans. Ind. Electron.*, vol. 60, no. 4, pp. 1492–1502, Apr. 2013.

[10] T. Chakraborty, D. Watson, and M. Rodgers, "Automatic generation control using an energy storage system in a wind park," *IEEE Trans. Power Syst*., vol. 33, no. 1, pp. 198–205, Jan. 2018.

[11] Q. Jiang, Y. Gong, and H. Wang, "A battery energy storage system dual-layer control strategy for mitigating wind farm fluctuations," *IEEE Trans. Power Syst*., vol. 28, no. 3, pp. 3263–3273, Aug. 2013.

[12] H. S. Krishnamoorthy, D. Rana, P. Garg, P. N. Enjeti, and I. J. Pitel, "Wind turbine generator–battery energy storage utility interface converter topology with medium-frequency transformer link," *IEEE Trans. Power Electron.*, vol. 29, no. 8, pp. 4146–4155, Aug. 2014.

[13] S. Tewari and N. Mohan, "Value of NAS energy storage toward integrating wind: Results from the wind to battery project," *IEEE Trans. Power Syst*., vol. 28, no. 1, pp. 532–541, Feb. 2013.

[14] F. Chang, O. Ilina, M. Lienkamp, and L. Voss, "Improving the overall efficiency of automotive inverters using a multilevel converter composed of low voltage si MOSFETS," *IEEE Trans. Power Electron*., vol. 34, no. 4, pp. 3586–3602, Apr. 2019.

[15] R. Karimi, D. Kaczorowski, A. Zlotnik, and A. Mertens, "Loss optimizing control of a multiphase interleaving DC-DC converter for use in a hybrid electric vehicle drivetrain," *in Proc. IEEE Energy Convers. Congr. Expo.*, 2016, pp. 1–8.

[16] M. Momayyezan, B. Hredzak, and V. G. Agelidis, "A load-sharing strategy for the state of charge balancing between the battery modules of integrated reconfigurable converter," *IEEE Trans. Power Electron*., vol. 32, no. 5, pp. 4056–4063, May 2017.

[17] J. G. Pinto, V. Monteiro, H. Goncalves, and J. L. Afonso, "Onboard reconfigurable battery charger for electric vehicles with traction-to-auxiliary mode," *IEEE Trans. Veh. Technol.*, vol. 63, no. 3, pp. 1104–1116, Mar. 2014.

[18] Qin Lei, Dong Cao, and Fang Zheng Peng, "Novel loss and harmonic minimized vector modulation for a current-fed quasi-z-source inverter in HEV motor drive application," *IEEE Trans. Power Electron*., vol. 29, no. 3, pp. 1344–1357, Mar. 2014.

[19] F. Michael, K. Mathias, S. Rohr, S. Schickrama, M. Sinninga, and M. Lienkamp, "An overview of costs for vehicle components, fuels, *Greenhouse Gas Emissions Total Cost Ownership Update 2017*," pp. 1–19, 2017. [Online]. Available: https://www.researchgate.net/publication/260339436_An_Overview_of_Costs_for_Vehicle_Components_Fuels_and_Greenhouse_Gas_Emissions

[20] B. Propfe, M. Redelbach, D. Santini, and H. Friedrich, "Cost analysis of plug-in hybrid electric vehicles including maintenance & repair costs and resale values," *World Elect. Veh. J.*, vol. 5, no. 4, pp. 886–895, Dec. 2012.

[21] Fang Zheng Peng, "A generalized multilevel inverter topology with self voltage balancing," *IEEE Trans. Ind. Appl.*, vol. 37, no. 2, pp. 611–618, Mar./Apr. 2001.

[22] L. M. Tolbert, Fang Zheng Peng, and T. G. Habetler, "Multilevel converters for large electric drives," *IEEE Trans. Ind. Appl.*, vol. 35, no. 1, pp. 36–44, Jan./Feb. 1999.

[23] F. Altaf and B. Egardt, "Comparative analysis of unipolar and bipolar control of modular battery for thermal and state-of-charge balancing," *IEEE Trans. Veh. Technol.*, vol. 66, no. 4, pp. 2927–2941, Apr. 2017.

[24] L. Maharjan, S. Inoue, H. Akagi, and J. Asakura, "State-of-charge (SOC)-balancing control of a battery energy storage system based on a cascade PWM converter," *IEEE Trans. Power Electron*., vol. 24, no. 6, pp. 1628–1636, Jun. 2009.

[25] K. Mozaffari, M. Amirabadi, and Y. Deshpande, "A single-phase inverter/rectifier topology with suppressed double-frequency ripple," *IEEE Trans. Power Electron.*, vol. 33, no. 11, pp. 9282–9295, Nov. 2018.

[26] Y. Shi, B. Liu, and S. Duan, "Low-frequency input current ripple reduction based on load current feedforward in a two-stage single-phase inverter," *IEEE Trans. Power Electron*., vol. 31, no. 11, pp. 7972–7985, Nov. 2016.

[27] J. Hicks-Garner *et al.*, "Cycle-life model for graphite-lifepo4 cells," *J. Power Sources*, vol. 196, no. 8, pp. 3942–3948, 2010.

[28] S. F. Schuster *et al.*, "Nonlinear aging characteristics of lithium-ion cells under different operational conditions," *J. Energy Storage*, vol. 1, pp. 44–53, Jun. 2015.

[29] A. Barré, B. Deguilhem, S. Grolleau, M. Gérard, F. Suard, and D. Riu, "A review on lithium-ion battery ageing mechanisms and estimations for automotive applications," *J. Power Sources*, vol. 241, pp. 680–689, Nov. 2013.

[30] J. Schmalstieg, S. Käbitz, M. Ecker, and D. U. Sauer, "A holistic aging model for Li(NiMnCo)O2 based 18650 lithium-ion batteries," *J. Power Sources*, vol. 257, pp. 325–334, Jul. 2014.

[31] W. Lee, B.-M. Han, and H. Cha, "Battery ripple current reduction in a three-phase interleaved dc-dc converter for 5 kW battery charger," *in Proc. IEEE Energy Convers. Congr. Expo.*, 2011, pp. 3535–3540.

[32] C. Liu, J. Wang, K. Colombage, C. Gould, B. Sen, and D. Stone, "Current ripple reduction in 4 kW LLC resonant converter based battery charger for electric vehicles," *in Proc. IEEE Energy Convers. Congr. Expo.*, 2015, pp. 6014–6021.

[33] D. B. W. W. Abeywardana, B. Hredzak, and V. G. Agelidis, "An input current feedback method to mitigate the dc-side low-frequency ripple current in a single-phase boost inverter," *IEEE Trans. Power Electron*., vol. 31, no. 6, pp. 4594–4603, Jun. 2016.

[34] D. B. W. Abeywardana, B. Hredzak, and V. G. Agelidis, "Battery-supercapacitor hybrid energy storage system with reduced low frequency input current ripple," *in Proc. Int. Conf. Renew. Energy Res. Appl.*, 2015, pp. 328–332.

[35] B. Liu *et al.*, "Input current ripple and grid current harmonics restraint approach for single-phase inverter under battery input condition in residential photovoltaic/battery systems," *IEEE Trans. Sustain. Energy*, vol. 9, no. 4, pp. 1957–1968, Oct. 2018.

[36] D. B. W. Abeywardana, B. Hredzak, and V. G. Agelidis, "Single-phase grid-connected LiFePO4 battery–supercapacitor hybrid energy storage system with interleaved boost inverter," *IEEE Trans. Power Electron.*, vol. 30, no. 10, pp. 5591–5604, Oct. 2015.

[37] C.-M. Lai, J. Teh, and Y.-H. Cheng, "An efficient active ripple filter for use in single-phase DC-AC conversion system," *in Proc. IEEE 8th Int. Conf. Awareness Sci. Technol.*, 2017, pp. 234–237.

[38] D. Patil and V. Agarwal, "Compact onboard single-phase ev battery charger with novel low-frequency ripple compensator and optimum filter design," *IEEE Trans. Veh. Technol.*, vol. 65, no. 4, pp. 1948–1956, Apr. 2016.

[39] H. V. Nguyen and D.-C. Lee, "Single-phase multifunctional onboard battery chargers with active power decoupling capability," *in Proc. IEEE Appl. Power Electron. Conf. Expo.*, 2018, pp. 3434–3439.

[40] O. Satilmis and E. Mese, "Investigating DC link current ripple and pwm modulation methods in electric vehicles," *in Proc. 3rd Int. Conf. Elect. Power Energy Convers. Syst.*, 2013, pp. 1–6.

[41] C. Ropeter, H. Wenzl, H. Beck, and E. A. Wehrmann, "The impact of microcycles on batteries in different applications," *in Proc. 18th Elect. Veh. Symp.*, 2001, pp. 1–12.

[42] T. Bulletin, "Ripple voltage and the affect on VRLA batteries."

[43] G. Fontes, C. Turpin, R. Saisset, T. Meynard, and S. Astier, "Interactions between fuel cells and power converters influence of current harmonics on a fuel cell stack," *in Proc. IEEE 35th Annu. Power Electron. Specialists Conf.*, 2004, pp. 4729–4735.

[44] S. Bala, T. Tengner, P. Rosenfeld, and F. Delince, "The effect of low frequency current ripple on the performance of a Lithium Iron Phosphate (LFP) battery energy storage system," *in Proc. IEEE Energy Convers. Congr. Expo.*, 2012, pp. 3485–3492.

[45] M. Uno and K. Tanaka, "Influence of high-frequency charge–discharge cycling induced by cell voltage equalizers on the life performance of lithium-ion cells," *IEEE Trans. Veh. Technol.*, vol. 60, no. 4, pp. 1505–1515, May 2011.

[46] T.-H. Kim *et al.*, "Analytical study on low-frequency ripple effect of battery charging," *in Proc. IEEE Veh. Power Propulsion Conf.*, 2012, pp. 809–811.

[47] H. Z. Z. Beh, G. A. Covic, and J. T. Boys, "Effects of pulse and DC charging on lithium iron phosphate (LiFePO4) batteries," *in Proc. IEEE Energy Convers. Congr. Expo.*, 2013, pp. 315–320.

[48] S. D. De Breucker, K. Engelen, R. D'hulst, and J. Driesen, "Impact of current ripple on Li-ion battery ageing," *World Elect. Veh. J.*, vol. 6, no. 3, pp. 532–540, Nov. 2013.

[49] M. J. Brand, M. H. Hofmann, S. S. Schuster, P. Keil, and A. Jossen, "The influence of current ripples on the lifetime of lithium-ion batteries," *IEEE Trans. Veh. Technol.*, vol. 67, no. 11, pp. 10438–10445, Nov. 2018.

[50] F. Chang, F. Roemer, M. Baumann, and M. Lienkamp, "Modelling and evaluation of battery packs with different numbers of paralleled cells," *World Elect. Veh. J.*, vol. 9, no. 1, pp. 1–15, Jun. 2018.

[51] "Specifications for NCR18650BD," Panasonic, Osaka, Japan, 2014.

[52] C. Campestrini, P. Keil, S. F. Schuster, and A. Jossen, "Ageing of lithium-ion battery modules with dissipative balancing compared with single-cell ageing," *J. Energy Storage*, vol. 6, pp. 142–152, May 2016.

[53] Z.-X. Zhang, X.-S. Si, C.-H. Hu, and M. G. Pecht, "A prognostic model for stochastic degrading systems with state recovery: application to li-ion batteries," *IEEE Trans. Rel*., vol. 66, no. 4, pp. 1293–1308, Dec. 2017.

[54] L. Tao, J. Ma, Y. Cheng, A. Noktehdan, J. Chong, and C. Lu, "A review of stochastic battery models and health management," *Renew. Sustain. Energy Rev.,* vol. 80, pp. 716–732, Dec. 2017.

[55] S. J. Moura, J. L. Stein, and H. K. Fathy, "Battery-health conscious power management in plug-in hybrid electric vehicles via electrochemical modeling and stochastic control," *IEEE Trans. Control Syst. Technol.*, vol. 21, no. 3, pp. 679–694, May 2013.

[56] F. H. Khan, L. M. Tolbert, and W. E. Webb, "Hybrid electric vehicle power management solutions based on isolated and nonisolated configurations of multilevel modular capacitor-clamped converter," *IEEE Trans. Ind. Electron.*, vol. 56, no. 8, pp. 3079–3095, Aug. 2009.

[57] L. A. Tolbert, Fang Zheng Peng, T. Cunnyngham, and J. N. Chiasson, "Charge balance control schemes for cascade multilevel converter in hybrid electric vehicles," *IEEE Trans. Ind. Electron.*, vol. 49, no. 5, pp. 1058–1064, Oct. 2002.

[58] S. F. Schuster, M. J. Brand, P. Berg, M. Gleissenberger, and A. Jossen, "Lithium-ion cell-to-cell variation during battery electric vehicle operation," *J. Power Sources*, vol. 297, pp. 242–251, Nov. 2015.

[59] M. Baumann, L. Wildfeuer, S. Rohr, and M. Lienkamp, "Parameter variations within Li-Ion battery packs – Theoretical investigations and experimental quantification," *J. Energy Storage*, vol. 18, pp. 295–307, Aug. 2018.

[60] L. W. Juang, P. J. Kollmeyer, A. E. Anders, T. M. Jahns, R. D. Lorenz, and D. Gao, "Investigation of the influence of superimposed AC current on lithium-ion battery aging using statistical design of experiments," *J. Energy Storage*, vol. 11, pp. 93–103, Jun. 2017

[61] Z. Zheng, K. Wang, L. Xu, and Y. Li, "A hybrid cascaded multilevel converter for battery energy management applied in electric vehicles," *IEEE Trans. Power Electron*., vol. 29, no. 7, pp. 3537–3546, Jul. 2014.

[62] M. Quraan, T. Yeo, P. Tricoli, and S. Korea, "Design and control of modular multilevel converters for battery electric vehicles," *IEEE Trans. Power Electron*., vol. 31, no. 1, pp. 507–517, Jan. 2015.

[63] M. Quraan, P. Tricoli, S. D Arco, and L. Piegari, "Efficiency assessment of modular multilevel converters for battery electric vehicles," *IEEE Trans. Power Electron*., vol. 32, no. 3, pp. 2041–2051, Mar. 2017.

[64] Brusa Elektronik, "Technical data and start-up of brusa motors," 2014.

[65] J. Merwerth, "The hybrid-synchronous machine of the new BMW i3 & i8, presentation on workshop university lund," 2014.

[66] B. Sarlioglu, C. T. Morris, D. Han, and S. Li, "Driving toward accessibility: a review of technological improvements for electric machines, power electronics, and batteries for electric and hybrid vehicles," *IEEE Ind. Appl. Mag.*, vol. 23, no. 1, pp. 14–25, Jan. 2017.

[67] J. Vedrana, S. Zeljko, and V. Zdravko, "Optimal control of induction motor using high performance frequency converter," *in Proc. 13th Int. Power Electron. Motion Control Conf.*, 2008, pp. 690–694.

[68] R. Prasad, C. Namuduri, and P. Kollmeyer, "Onboard unidirectional automotive G2V battery charger using sine charging and its effect on li-ion batteries," *in Proc. IEEE Energy Convers. Congr. Expo.*, 2015, pp. 6299–6305

[69] L. W. Juang, P. J. Kollmeyer, A. E. Anders, T. M. Jahns, R. D. Lorenz, and D. Gao, "Investigation of the influence of superimposed AC current on lithium-ion battery aging using statistical design of experiments," *J. Energy Storage*, vol. 11, pp. 93–103, Jun. 2017